Journal of Molecular Catalysis A: Chemical 331 (2010) 130–136

Contents lists available at ScienceDirect

Journal of Molecular Catalysis A: Chemical

journal homepage: www.elsevier.com/locate/molcata

Influence of interaction between CeO_2 and USY on the catalytic performance of CeO_2–USY catalysts for deep oxidation of 1,2-dichloroethane

Qinqin Huang, Xiaomin Xue, Renxian Zhou*

Institute of Catalysis, Zhejiang University, Hangzhou 310028, PR China

ARTICLE INFO

Article history:
Received 25 March 2010
Received in revised form 12 July 2010
Accepted 12 August 2010
Available online 20 August 2010

Keywords:
CeO_2–USY catalyst
Synergy
Preparation method
Durability

ABSTRACT

Three supported CeO_2–USY catalysts were prepared by different CeO_2 loading methods and evaluated for the deep oxidation of 1,2-dichloroethane (DCE). All the catalysts were characterized by X-ray diffraction (XRD), high resolution transmission electron microscopy (HRTEM), ammonia temperature-programmed desorption (NH_3-TPD), diffuse reflectance infrared spectra of pyridine adsorption (DRIFT), hydrogen temperature-programmed reduction (H_2-TPR), oxygen storage capacity complete (OSCC) and X-ray photoelectron spectroscopy (XPS) techniques. The results show that a strong synergy effect occurs in the CeO_2–USY catalysts prepared by impregnation method and mechanical grinding of USY and $Ce(NO_3)_3{\cdot}6H_2O$. Moreover, higher dispersion of CeO_2 species, better mobility of oxygen species of the catalysts as well as better catalytic activity for DCE decomposition are obtained over these two catalysts. All the CeO_2–USY catalysts show a high selectivity towards the formation of HCl. In addition, the CeO_2–USY catalyst prepared by impregnation method maintains a high conversion in the 100 h test of DCE decomposition.

1. Introduction

Chlorinated volatile organic compounds (CVOCs) are released to the atmosphere in flue gases from a variety of industrial processes. Such compounds are well known to be toxic to human beings and to be involved in the formation of photochemical smog as well as the depletion of ozone layer in the stratosphere [1]. Catalytic oxidation for removal of CVOCs has received increasing attention among the various disposal methods. It is usually carried out at relatively low temperature (<773 K) and produces less harmful products via complete oxidation of the chlorinated hydrocarbons into CO_2 and HCl [2,3]. Therefore, it is more efficient especially for low concentration of CVOCs compared to thermal incineration [4].

In recent years, more and more consideration has been given to zeolite catalysts with strong acid sites, which play a key role in controlling the decomposition of chlorinated compounds [5,6]. However, easy coke deposition on zeolite limits its utilization [7,8]. In order to improve the catalytic activity as well as the stability, metal-loaded or dealumination-treatment zeolite catalysts have been the potentially alternative catalysts for end-of-pipe pollution control due to its high catalytic activity, favorable selectivity towards desired reaction products and good durability for CVOC decomposition [9–11].

It is well known that the preparation method has a significant influence on the physicochemical properties of the catalysts, such as dispersion of active phases, structure of the catalysts and redox property of the catalysts, which in turn affect the catalytic performance of the catalysts [12,13]. Compared with ion-exchanged zeolite, impregnated silver-loaded zeolite shows a lower uptake capacity of butyl acetate ascribed to the changes in the pore characteristics and available surface for adsorption [14]. Ce–SBA-15 synthesized by a direct hydrothermal method appears more suitable for preparing supported cobalt catalysts comparing with CeO_2/SBA-15 prepared by an impregnation method, although Co supported on Ce–SBA-15 catalysts destroy the ordered mesoporous structure with partial blockage of pores [15]. In terms of the influence of the electronegativity of charge-compensating cation (Na^+, Cs^+ and H^+) on the Pd particles, Pd dispersion, PdO reducibility and the adsorption energies of VOCs, various catalytic activities for total oxidation of propene and toluene can be rationalized over Pd supported on ion-exchanged BEA and FAU zeolites [16]. Although the influence of preparation method on the characteristics as well as the catalytic behavior of the catalysts has been reported in a lot of literature, systematic researches are limited up to now.

In this study, three supported CeO_2–USY catalysts were prepared by different CeO_2 loading methods and evaluated for DCE oxidation. The catalysts were characterized by XRD, HRTEM, NH_3-TPD, DRIFT, H_2-TPR, OSCC and XPS techniques. The aim of this study is to have a discussion about the influence of interaction between CeO_2 and USY on the characteristics and the catalytic performance

* Corresponding author. Tel.: +86 571 88273290; fax: +86 571 88273283.
E-mail address: zhourenxian@zju.edu.cn (R. Zhou).

1381-1169/$ – see front matter.
doi:10.1016/j.molcata.2010.08.017

of CeO_2–USY catalysts. In addition, the durability of the catalyst has also been examined.

2. Experimental

2.1. Catalysts preparation

Raw USY zeolites were supplied by HUAHUA Corp., Wenzhou, China and used after calcined at 823 K for 2 h. Pure CeO_2 was prepared by calcination of $Ce(NO_3)_3{\cdot}6H_2O$ at 823 K for 2 h. Three CeO_2–USY catalysts were prepared by different CeO_2 loading methods. CeO_2–USY-IM was prepared by non-calcined USY impregnated with $Ce(NO_3)_3{\cdot}6H_2O$ (AR, 98.0%) solution. CeO_2–USY-M1 was prepared by mechanical grinding of non-calcined USY with $Ce(NO_3)_3{\cdot}6H_2O$. CeO_2–USY-M2 was prepared by mechanical grinding of non-calcined USY with CeO_2 (obtained from calcination of $Ce(NO_3)_3{\cdot}6H_2O$ at 823 K for 2 h). All the catalysts were dried at 373 K for 2 h, and then calcined in air at 623 K for 0.5 h and further at 823 K for 2 h. All the obtained catalysts were pressed into pellets, crushed and sieved to 40–60 meshes. The mass ratio of CeO_2 to USY is 1:8 for all the CeO_2–USY catalysts.

2.2. Catalytic activity tests

Catalytic activity tests were carried out in a micro-reactor (quartz glass, 6 mm i.d., GC 1690, China). The feed gas composition was: [DCE] = ~1000 ppm with air as balance, and the operating condition was: GHSV = 15,000 h^{-1} with a total flow of 75 mL min^{-1}. The durability of the catalyst was performed at 573 K for 100 h with GHSV = 15,000 h^{-1} and [DEC] = ~1000 ppm.

The trend of chlorinated products (HCl and Cl_2) was detected under the catalytic activity tests condition ([DCE] = 1000 ppm, GHSV = 15,000 h^{-1}). The catalysts were heated at a rate of 5 °C min^{-1} from 373 to 823 K. The products were analyzed on-line over a mass spectrometer apparatus (HIDEN QIC-20).

2.3. Catalysts characterization

The X-ray diffraction (XRD) measurement was performed on an ARL X'TRA X-ray Diffractometer (Thermo Electron Corporation, USA), with Cu Kα radiation at 40 kV and 40 mA in a scanning range of 3–70° (2θ).

The high resolution transmission electron microscopy (HRTEM) was carried out on JEM-2010 apparatus operated at 200 kV.

The ammonia temperature-programmed desorption (NH_3-TPD) was performed in a quartz fixed-bed micro-reactor equipped with TCD. Prior to adsorption of ammonia, the catalyst (100 mg) was pre-treated in a N_2 stream (99.99%, 35 mL min^{-1}) at 773 K for 0.5 h. After being cooled down to 373 K, the catalyst was exposed to a flow (30 mL min^{-1}) of 20 vol.% NH_3/N_2 mixture for 30 min, and then treated in a N_2 flow for 1 h in order to remove physically bound ammonia. Finally, desorption performance was carried out in a N_2 flow (40 mL min^{-1}) from 100 to 873 K at a heating rate of 10 K min^{-1}. All these profiles were simulated by Gaussian functions.

The diffuse reflectance infrared spectra of pyridine adsorption (DRIFT) were obtained with a Nicolet Nexus 470 spectrometer (NICOLET Corporation, USA). All spectra were recorded in the range 4000–1300 cm^{-1} with a 2 cm^{-1} resolution. After the catalyst was evacuated at 573 K at 10^{-5} Pa for 4 h, pyridine vapor was admitted at room temperature until the catalyst surface was saturated. Pyridine was desorbed until a pressure of 10^{-5} Pa to ensure that there was no more physisorbed pyridine. The spectra of adsorbed pyridine were then measured. Different spectra were obtained by subtracting the spectrum of the dehydrated catalysts from the spectra obtained after pyridine adsorption.

The hydrogen temperature-programmed reduction (H_2-TPR) was performed in a quartz fixed-bed micro-reactor equipped with TCD, using a 5 vol.% H_2/Ar mixture. After the catalysts were pre-treated in air at 573 K for 0.5 h, the reduction was carried out from 100 to 1073 K at a heating rate of 10 K min^{-1}.

The oxygen storage capacity complete (OSCC) was measured using pulse injection technique with a CHEMBET-3000 as the analytical device. The sample was first reduced with a flow of 10 mL min^{-1} H_2 at 823 K for 1 h, then cooled to the testing temperature and purged by helium stream. The OSCC was measured by pulse injection of oxygen into the sample bed until no consumption of oxygen could be detected by a TCD. The amount of oxygen consumed during the re-oxidation stage is referred as OSCC and was expressed as μmol of O per gram of catalyst (μmol [O]/g). All the gases employed in the experiment were high-purity (99.99%).

The coke content was measured in a Thermogravimetric Analyzer TGA (Perkin Elmer Inc., USA). After the pre-treatment in a N_2 flow (99.99%, 30 mL min^{-1}) at 393 K for 0.5 h, the used catalyst was further heated up to 1073 K at a rate of 10 K min^{-1} in a synthetic flow (40% O_2 + 60% N_2, 99.99%, 60 mL min^{-1}).

The X-ray photoelectron spectroscopy (XPS) analysis was recorded with a PHI5000c spectrometer at 1486.6 eV and 12.5 kV using Al Kα radiation. The samples were pressed into thin discs and mounted on a sample rod placed in a pre-treatment chamber. The spectra of Ce 3d and Al 2p levels were recorded. All the binding energy (BE) values were calibrated using the C 1s peak at 284.8 eV. The relative abundance of Ce^{4+} presenting in the catalyst is assessed through the calculation of the percentage of the area under the Ce^{4+} u‴ peak (BE = 917 eV) relative to the total area under the Ce 3d spectral envelope using the method proposed by Shyu et al. [17].

3. Results and discussion

3.1. Catalytic activity results

The catalytic activity of CeO_2, USY and CeO_2–USY catalysts is presented in Fig. 1. As shown in Fig. 1(A), CeO_2–USY-IM and CeO_2–USY-M1 show much higher DCE conversion compared with CeO_2 and USY. It suggests that a strong interaction between CeO_2 and USY zeolite occurs in CeO_2–USY catalysts prepared by impregnation method and USY mechanical grinding with $Ce(NO_3)_3{\cdot}6H_2O$, which is beneficial to the decomposition of DCE. Due to the rather weak interaction between CeO_2 and USY in CeO_2–USY-M2 prepared by USY mechanical grinding with CeO_2, DCE conversion over the catalyst is similar to that over USY. On the basis of T_{90} (temperature at which 90% conversion is achieved), the catalytic activity decreases in the order of CeO_2–USY-IM (518 K) ≈ CeO_2–USY-M1 (522 K) > CeO_2–USY-M2 (573 K) > USY (583 K) > CeO_2 (607 K).

CH_3Cl, C_2H_3Cl, CH_3CHO and CH_3COOH are common by-products and intermediates during DCE decomposition. The characteristic curve of CH_3Cl resulted from the DCE cracking is presented in Fig. 1(B). There is little CH_3Cl produced over CeO_2, while large concentration of CH_3Cl is detected over USY due to the existence of plentiful strong acid sites in USY zeolite [18,19]. With the introduction of CeO_2 to USY, the temperature at which CH_3Cl reaches the maximum value is evidently lowered for CeO_2–USY-IM and CeO_2–USY-M1 in comparison with that for USY and CeO_2–USY-M2. It is supposed that the strong interaction between CeO_2 and USY promotes the cracking of DCE.

C_2H_3Cl is the main intermediate produced during decomposition of DCE via dehydrochlorination [20,21]. The temperature–concentration relationship of C_2H_3Cl is presented in Fig. 1(C). Within the temperature range of 433–613 K in our study, the relation between the DCE decline and C_2H_3Cl incre-

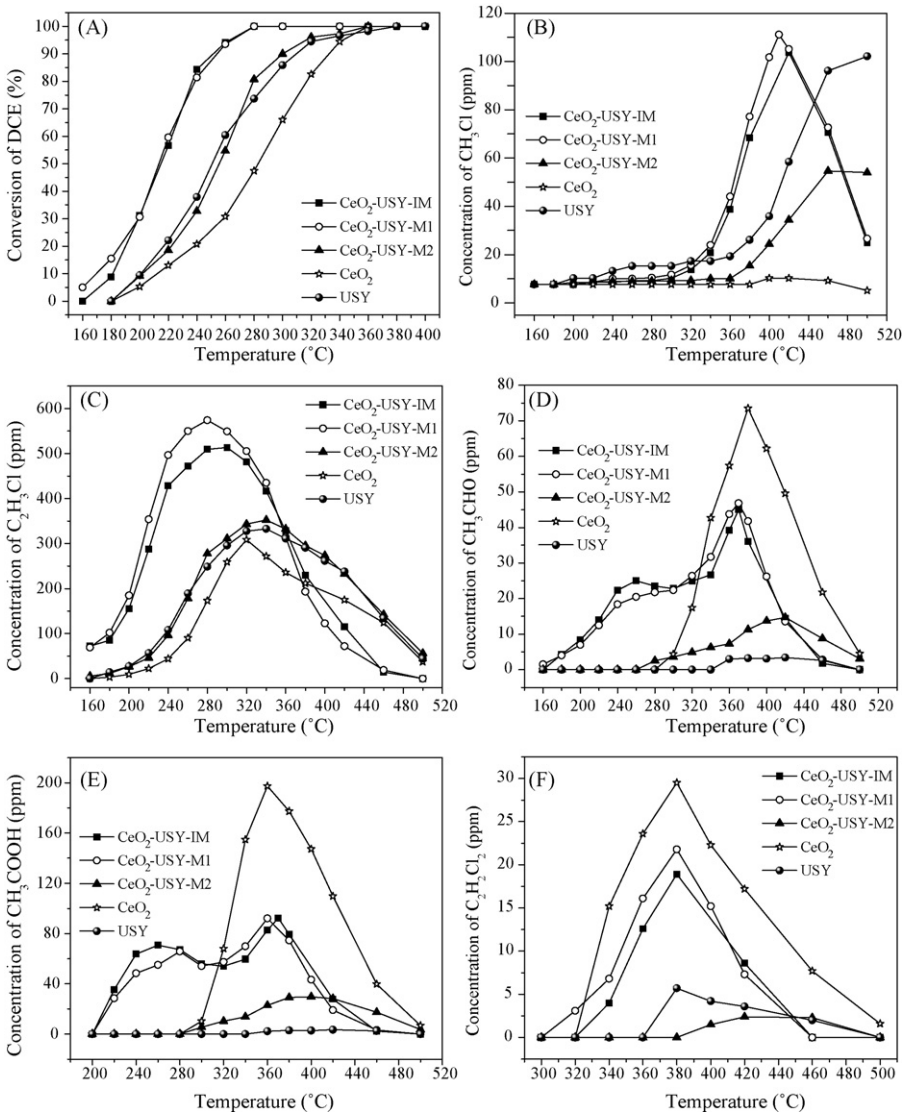

Fig. 1. The catalytic activity of CeO_2, USY and CeO_2–USY catalysts: (A) conversion of DCE; (B) concentration of CH_3Cl; (C) concentration of C_2H_3Cl; (D) concentration of CH_3CHO; (E) concentration of CH_3COOH; (F) concentration of $C_2H_2Cl_2$.

ment is almost linear. Also, the maximum concentration for C_2H_3Cl occurs at the temperature when DCE is completely consumed. The maximum concentration of C_2H_3Cl over each catalyst follows the order of CeO_2–USY-M1 (574 ppm) > CeO_2–USY-IM (514 ppm) > CeO_2–USY-M2 (352 ppm) > USY (333 ppm) > CeO_2 (309 ppm).

As shown in Fig. 1(D) and (E), nearly no CH_3CHO or CH_3COOH is examined over USY, while large concentration of these two intermediates is detected over CeO_2–USY catalysts and CeO_2. It is caused by the presence of oxygen species in these catalysts except for USY, since CH_3CHO and CH_3COOH are produced via further oxidation of C_2H_3Cl [21]. With regard to the concentration of these two intermediates produced over each catalyst, more CH_3CHO and CH_3CHOOH are detected over pure CeO_2 than that over CeO_2–USY-M2 with a similar peak-temperature at ca. 673 K when the maximum concentration of these two intermediates is achieved, which can be due to the much more oxygen species contained in pure CeO_2. The concentration of the intermediates is also higher over CeO_2–USY-IM and CeO_2–USY-M1 than that over CeO_2–USY-M2. Moreover, it is noticeable that two maximum concentrations of these two intermediates (one at ca. 533 K and the other at ca. 653 K) are observed on these two catalysts and the temperature at which the second maximum concentration achieved is similar to that (673 K) over pure CeO_2 and CeO_2–USY-M2. We speculate that such an interesting phenomenon may be related to the different mobility of oxygen species among CeO_2–USY catalysts prepared by different methods. Additionally, an unfavorable product $C_2H_2Cl_2$ is also detected during catalytic oxidation of DCE (Fig. 1(F)). However, the concentration is always below 30 ppm.

The common chlorinated products (HCl and Cl_2) during the deep oxidation of DCE are examined. Transformations of HCl and Cl_2 with temperature on CeO_2–USY catalysts are shown in Fig. 2. It is obviously seen that HCl is the major chlorinated product, which increases obviously along with the increasing temperature and decreases slightly above 400 °C. It suggests that all the catalysts show a high selectivity towards HCl. According to the literature reported, the hydroxyls in the zeolite structure largely promote the formation of HCl by the Deacon reaction, especially in the combustion of compounds with a low H/Cl ratio [22,23]. What is more, HCl is the preferred chlorinated decomposition by-product instead

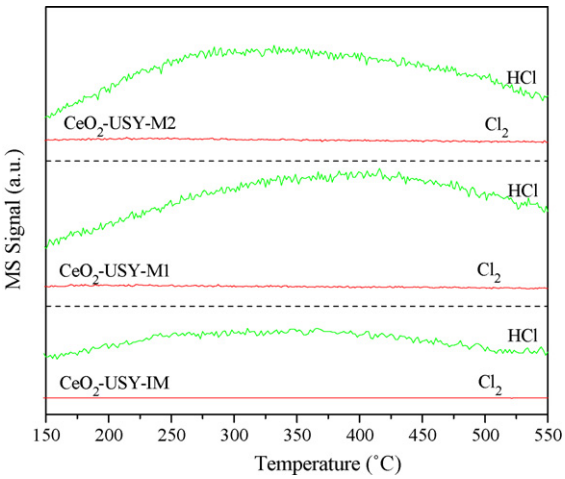

Fig. 2. The transformations of chlorinated by-products during DCE oxidation over CeO_2–USY catalysts.

of Cl_2, since it is less toxic and can be readily removed from the effluent stream by downstream aqueous scrubbing.

3.2. Catalysts characterization results

3.2.1. Dispersion of CeO_2 species on USY zeolite

XRD patterns of CeO_2, USY and CeO_2–USY catalysts are shown in Fig. 3. It can be seen that intense diffraction peaks ascribed to

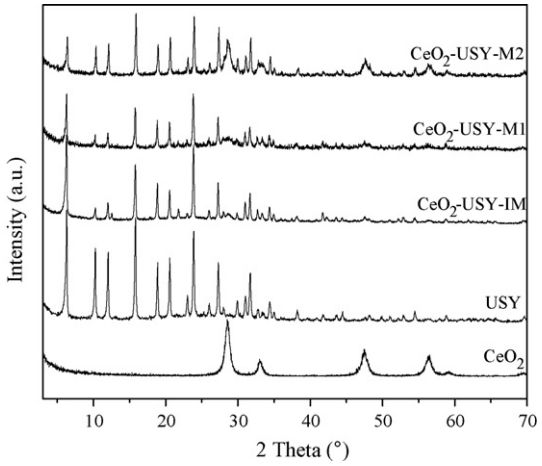

Fig. 3. XRD patterns of CeO_2, USY and CeO_2–USY catalysts.

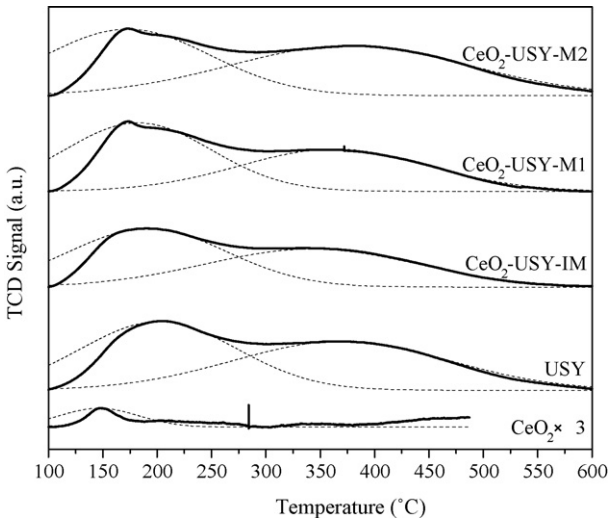

Fig. 5. NH_3-TPD profiles of CeO_2, USY and CeO_2–USY catalysts.

the fluorite structure of CeO_2 [24] are observed on CeO_2–USY-M2, while the intensity of these peaks is much weaker on CeO_2–USY-IM and CeO_2–USY-M1. It indicates that both impregnation and mechanical grinding of $Ce(NO_3)_3{\cdot}6H_2O$ and USY bring in strong interaction between CeO_2 and USY, which results in a high dispersion of CeO_2 species on USY. The results of HRTEM further confirm the dispersion of CeO_2 species on USY zeolite. As shown in Fig. 4, the aggregation of CeO_2 species more obvious over CeO_2–USY-M2, indicating a poorer dispersion of CeO_2 on USY. As a result, the better catalytic activity of CeO_2–USY-IM and CeO_2–USY-M1 may be due to the high dispersion of CeO_2 species, which is a key factor conditioning the catalytic performance [25]. Moreover, compared with the XRD patterns of USY and CeO_2–USY catalysts, the strong interaction between CeO_2 and USY does not lead to the large distortion of the ordered silica structure.

3.2.2. Acidity

NH_3-TPD profiles of CeO_2, USY and CeO_2–USY catalysts are given in Fig. 5. Only one desorption peak (about 423 K) with rather weak signal is observed on CeO_2, which indicates that only a few amount of weak acid sites exists in CeO_2. Similar profiles are observed in USY and CeO_2–USY catalysts. The first desorption peak ascribed to weak acid sites appears at the range of 448–548 K, and the second one assigned to strong acid sites exists at the range of 623–723 K. With the introduction of CeO_2, the peak-temperature of the first desorption peak evidently shifts to lower temperature for all the CeO_2–USY catalysts, while that of the second peak changes a little.

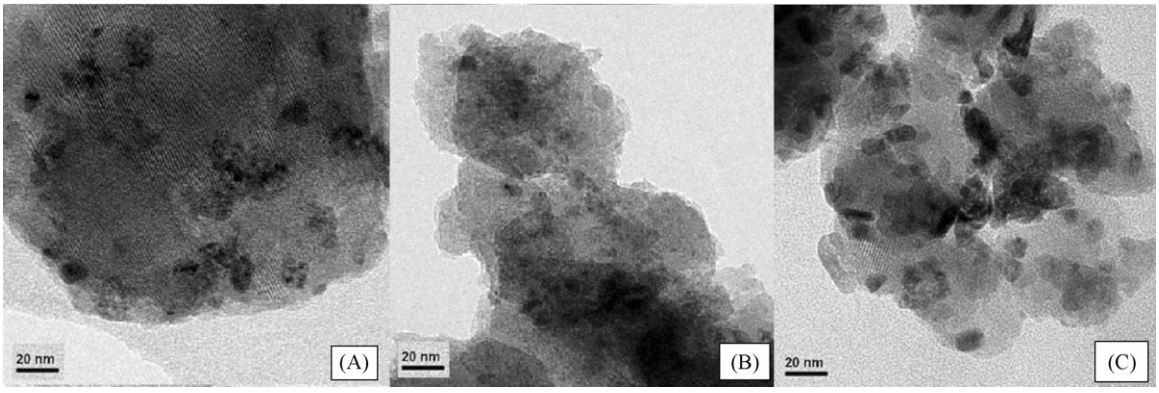

Fig. 4. HRTEM images of CeO_2–USY catalysts: (A) CeO_2–USY-IM; (B) CeO_2–USY-M1; (C) CeO_2–USY-M2.

Table 1
Acidity distribution of USY, CeO_2 and CeO_2–USY catalysts.

	Total acidity (mmol NH_3/g cat)	Weak acidity (mmol NH_3/g cat)	Strong acidity (mmol NH_3/g cat)
USY	1.030	0.502	0.528
CeO_2–USY-IM	0.750	0.382	0.368
CeO_2–USY-M1	0.836	0.443	0.393
CeO_2–USY-M2	0.928	0.407	0.521
CeO_2	0.020	0.020	0
CeO_2–USY-IM-used	0.617	0.344	0.273

Taking the intensity of these desorption peaks into consideration, it is obviously observed that the intensity of the peak attributed to weak acid sites is similar to each other for USY and all the CeO_2–USY catalysts. However, the intensity of strong acid sites is weaker for CeO_2–USY-IM and CeO_2–USY-M1 than that for USY and CeO_2–USY-M2. As shown in Table 1, the introduction of CeO_2 leads to an obvious reduction of total acidity over CeO_2–USY-IM and CeO_2–USY-M1, which affects more on strong acidity than on weak acidity.

It is well known that diffuse reflectance infrared spectra (DRIFT) of pyridine adsorbed mainly shows the nature of the acid sites, discriminating between Brønsted and Lewis acid sites. Therefore, the diffuse reflectance infrared spectra of pyridine adsorbed on USY and CeO_2–USY catalysts are also determined and shown in Fig. 6. On all the samples after pyridine adsorbed at room temperature (Fig. 6(A)), distinct bands are obviously observed. They are ascribed to hydrogen bonded pyridine, Lewis bound pyridine, Brønsted bound pyridine and pyridine associated with Brønsted and Lewis acid sites, respectively [26–29]. The intensity of all the bands are slightly weaker on CeO_2–USY-IM and CeO_2–USY-M1 than that on CeO_2–USY-M2 and USY. It is known that DRIFT spectra obtained at a relatively high temperature are usually used as a determination of strong acid sites. It is evidently seen that there are fewer strong acid sites, both Lewis acidity and Brønsted acidity, on CeO_2–USY-IM and CeO_2–USY-M1 (Fig. 6(B)). Therefore, according to the acidity characterizations, we suggest that the strong interaction between CeO_2 and USY over CeO_2–USY-IM and CeO_2–USY-M1 weakens the acidity of the catalysts, which influences more on strong acid sites than on weak acid sites.

According to the previous research, the mechanism of the oxidation of DCE is known as follows [21]: The decomposition occurs firstly through dehydrochlorination of DCE into vinyl chloride in the presence of Lewis acid sites. This intermediate can be attacked by nucleophilic oxygen species from the catalyst to form chlorinated alkoxide species, which readily decompose to generate

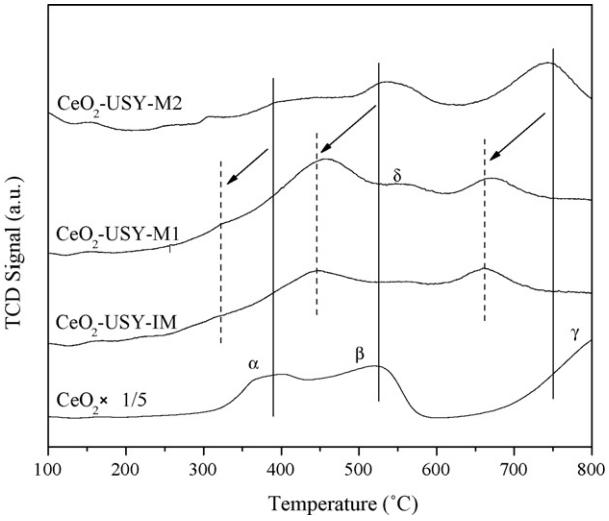

Fig. 7. H_2-TPR profiles of CeO_2 and CeO_2–USY catalysts.

acetaldehyde through dehydrochlorination in the presence of protonic acid sites, acetates and CO_x. Combining with the results of C_2H_3Cl production, it is speculated that the strong interaction between CeO_2 and USY in CeO_2–USY-IM and CeO_2–USY-M1 promotes the dehydrochlorination of DCE on Lewis acid sites at relatively lower temperature range. However, the relatively smaller amount of protonic acid sites (Brønsted acid sites) on CeO_2–USY-IM and CeO_2–USY-M1 inhibits the further dehydrochlorination of C_2H_3Cl. Thus, more C_2H_3Cl is produced on these two catalysts in DCE destruction.

3.2.3. Redox properties

Cerium oxide is well known for its facile reducibility compared to other fluorite-type oxides [30]. H_2-TPR profiles of CeO_2 and CeO_2–USY catalysts prepared by different CeO_2 loading ways are displayed in Fig. 7. Evidently, three reduction peaks are observed on pure CeO_2. Peaks α and β detected below 873 K are ascribed to the reduction of surface and sub-surface oxygen, and peak γ observed above 873 K is assigned to the reduction of bulk oxygen [24]. With the introduction of CeO_2, the reducibility of CeO_2–USY-M2 is similar to pure CeO_2 except that the reduction peak of bulk oxygen shifts to lower temperature. In the case of CeO_2–USY-IM and CeO_2–USY-M1, the reduction peaks of both surface oxygen and bulk oxygen evidently shift to lower temperature range. The peak intensity ratio (surface/bulk) is higher than that for CeO_2–USY-M2, which indicates the strong interaction between CeO_2 and USY enhances

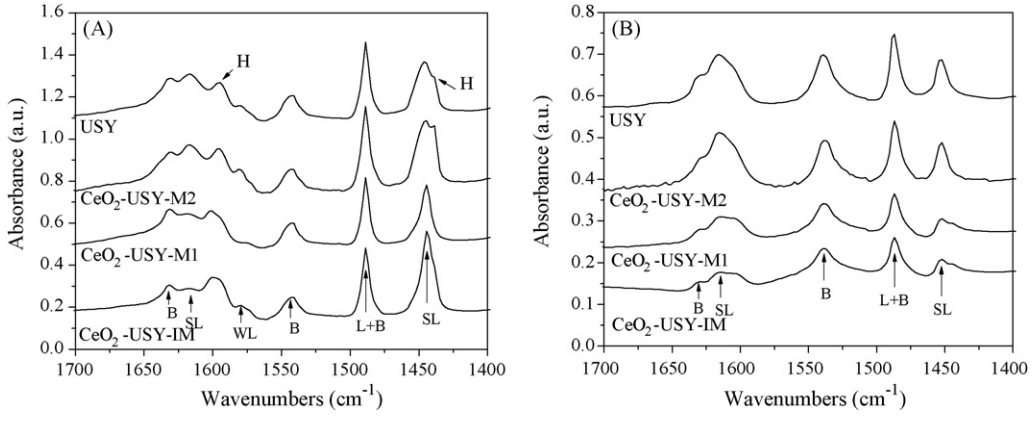

Fig. 6. DRIFT spectra of pyridine adsorbed on USY and CeO_2–USY catalysts: (A) room temperature; (B) 300 °C. H: hydrogen bonded pyridine; B: Brønsted bound pyridine; L: Lewis bound pyridine.

the oxygen mobility within CeO_2–USY-IM and CeO_2–USY-M1 compared with CeO_2–USY-M2 [31]. Moreover, the broad peak observed within the temperature 573–873 K with also demonstrates the good redox properties for CeO_2–USY-IM and CeO_2–USY-M1 [32]. One more weak signal, signed as peak δ, is detected between 823 and 873 K. It may be attributed to the reduction of bulk oxygen in CeO_2 species with small particles, since high dispersion of CeO_2 species is observed based on the XRD results. In addition, oxygen storage capacity complete (OSCC) technique has been widely used to characterize the oxygen storage/release behavior of ceria-based materials. According to our test, the OSCC is 52, 44 and 40 μmol [O]/g for CeO_2–USY-IM, CeO_2–USY-M1 and CeO_2–USY-M2, respectively. Although there is no direct correlation between the reducibility and the OSCC of the catalysts, the results above suggest that the strong interaction between CeO_2 and USY improves the mobility of the oxygen species, which is beneficial to the migration of oxygen from bulk to surface and increment of the oxygen storage capacity of the catalysts.

Combining with production of CH_3CHO and CH_3COOH, it is deduced that the redox properties of the catalysts has a significant effect on the production of CH_3CHO and CH_3COOH. It is known that CH_3CHO and CH_3COOH are the products via further oxidation of C_2H_3Cl, which relates closely to the concentration of active oxygen species in the catalyst as well as the mobility of the oxygen species [21]. With regard to the concentration of CH_3CHO and CH_3COOH, more CH_3CHO and CH_3COOH produced over CeO_2–USY-IM and CeO_2–USY-M1 than that over CeO_2–USY-M2 can be due to the better migration of the oxygen species from the bulk to surface in the catalysts. In the case of pure CeO_2, the largest concentration of CH_3CHO and CH_3COOH produced is due to the fact that the concentration of oxygen species in pure CeO_2 is evidently higher than that in the other catalysts. In addition, it is speculated that the existence of two maximum concentrations of CH_3CHO and CH_3COOH over CeO_2–USY-IM and CeO_2–USY-M1 relates to the much better mobility of the oxygen species in the two catalysts, especially the surface oxygen species, which may be the cause of the existence of the first maximum concentration.

3.3. Durability of CeO_2–USY-IM

The behavior of CeO_2–USY-IM in the oxidation of DCE as conversion vs. time on stream is presented in Fig. 8. It is obviously seen that the conversion of DCE maintains at 100% (573 K, 15,000 h^{-1}) within the whole time range (100 h), suggesting that the catalyst exhibits good durability during the DCE decomposition. It has been reported that the deactivation of zeolite catalysts is mainly caused by coke deposition [7,33]. According to the TGA results, the low coke content (1.1%) of used CeO_2–USY-IM may be one of the reasons that high conversion of DCE is maintained during the whole test. It is also known that the deactivating effect of coke is dependent on the pore structure of zeolites to certain extent [34–36]. It is supposed that low coke deposition of CeO_2–USY-IM may be related to its three-dimensional channel structure, the uniform channel size (0.76 nm) and super-cage structure, which easily allows the inlet of feed molecules as well as the outlet of the product molecules. In addition, the better oxygen delivery ability of the catalyst promoted by the synergy effect between CeO_2 and USY, which inhibits the coke deposition during DCE destruction, may also be a factor to the low coke content of CeO_2–USY-IM. The acidity of the used catalyst (listed in Table 1) shows an evident loss compared with that of the fresh catalyst. Moreover, the decrease in strong acid sites (25.8%) is much greater than that in weak acid sites (9.9%). As presented in Fig. 8(B), the temperature at which DCE is completely converted over used catalyst is the same as that over the fresh catalyst. However, the catalytic activity of used catalyst decreases about 3–12% at low temperature range compared with that of the fresh catalyst. It may be due to the reduction of acid sites and coke deposition in the used catalyst.

Table 2
Binding energy and relative abundance of elements in CeO_2–USY-IM.

CeO_2–USY-IM	Binding energy (eV)		Relative abundance of Cl, Al and Si (%)		
	O 1s	Al 2p	Cl 2p	Al 2p	Si 2p
Fresh	532.0	74.5	0.19	53.75	46.06
Used	532.1	74.7	1.31	50.73	47.96

The oxidation states and relative abundance of surface species for fresh or used CeO_2–USY-IM catalyst were characterized by XPS techniques. XPS spectra of Ce 3d and Al 2p are presented in Fig. 9. The binding energy (BE) of Al 2p and O 1s, and the relative abundance of elements Cl, Al and Si are listed in Table 2. From Fig. 9(A), it can be seen that the coexistence of Ce(III) and Ce(IV) oxidation states can be clearly distinguished in the Ce 3d spectra of the fresh and used catalysts [37–39]. The peak ascribed to Ce^{3+} is more visible in the used catalyst. According to the calculation, the relative abundance of Ce^{4+} is 9.87% and 6.39% in the fresh and used catalyst, respectively. In addition, element Cl (1.31%) is detected after the 100 h reaction, which demonstrates that element Cl enters into the framework of the catalyst. The reduction of the Ce^{4+} content and the increment of Cl content may be due to the formation of non-active species such as CeOCl and $CeCl_3$ [40].

As shown in Fig. 9(B) and Table 2, the core level peak corresponding to Al 2p is observed at about 74.5 and 74.7 eV on the fresh and used catalyst, respectively. The intensity of the peak decreases on the used catalyst compared with that on fresh catalyst and the reduction of Al content is clearly seen in Table 2. Al–O bonds of the zeolites used in the oxidation chlorinated VOCs can be attacked by the reaction product HCl [41] resulting in the for-

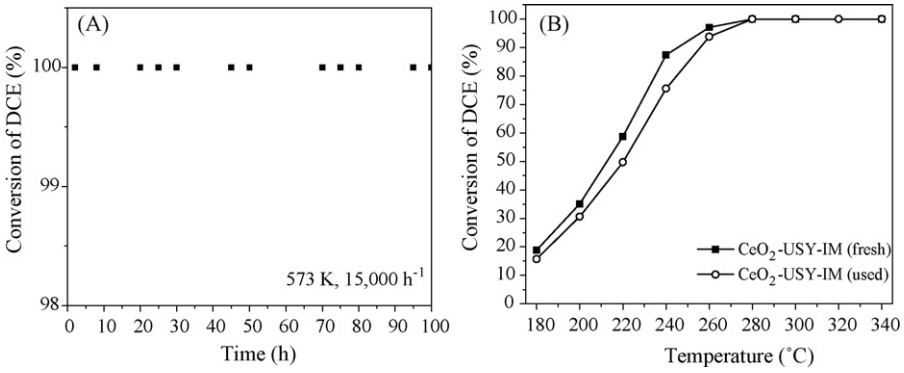

Fig. 8. (A) The catalytic behavior of CeO_2–USY-IM as a function of time on stream; (B) light-off curves of DCE oxidation over CeO_2–USY-IM fresh/used catalyst.

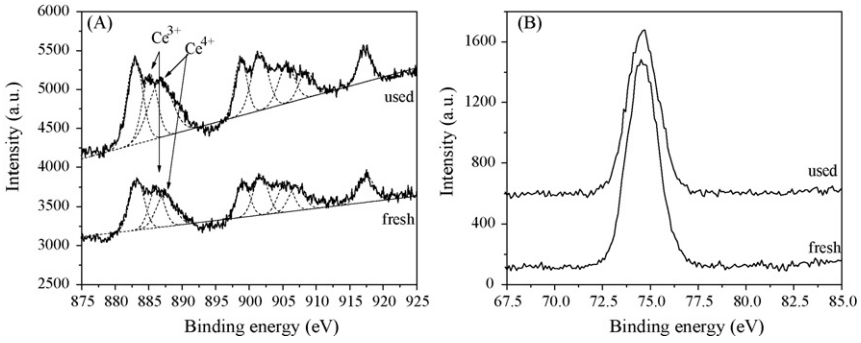

Fig. 9. XPS spectra of (A) Ce 3d and (B) Al 2p of CeO_2–USY-IM.

mation of volatile $AlCl_3$ molecules which takes away Al atoms from the zeolite [42–44]. In addition, the break of Al–O bond may be the cause of the reduction in the acidity of the catalyst.

It is reported that the O 1s BE for cerium oxides can shift from 529.6 to 530.3 eV [45]. The O 1s BE at about 530 eV belongs most likely to a defect-oxide or a hydroxyl-like group, which have higher mobility. They can actively take part in the oxidation process and greatly contribute to the catalyst activity [46]. As listed in Table 2, the O 1s BE is almost the same in the fresh and used catalyst. It is an evidence for the good durability of the catalyst during DCE decomposition.

4. Conclusion

Three supported CeO_2–USY catalysts were prepared by different loading methods of CeO_2 on USY zeolite and evaluated in the course of DCE deep oxidation. According to the study, we conclude that the CeO_2 loading method on USY zeolite significantly affects the interaction between CeO_2 and USY zeolite. A strong synergy effect occurs in the CeO_2–USY catalyst prepared by either impregnation method or mechanical grinding of USY and $Ce(NO_3)_3{\cdot}6H_2O$, which improves the dispersion of CeO_2 species and the migration of the oxygen species from the bulk to surface, and thus promotes the catalytic activity for DCE decomposition. Additionally, all the CeO_2–USY catalysts show a high selectivity to HCl formation. The good durability of CeO_2–USY-IM catalyst during the 100 tests of DCE decomposition is related to its three-dimensional channel structure, the uniform channel size and super-cage structure as well as the better deeper oxidation ability.

Acknowledgements

We gratefully acknowledge the financial supports from the Ministry of Science and Technology of China (No. 2004 CB 719504) and Nature Science Foundation of China (No. 20577043).

References

[1] J.R. González-Velasco, R. López-Fonseca, A. Aranzabal, J.I. Gutiérrez-Ortiz, P. Steltenpohl, Appl. Catal. B 24 (2000) 233–242.
[2] R. López-Fonseca, A. Aranzabal, P. Steltenpohl, J.I. Gutiérrez-Ortiz, J.R. González-Velasco, Catal. Today 62 (2000) 367–377.
[3] J. Janas, R. Janik, T. Machej, E.M. Serwicka, E. Bielańska, Catal. Today 59 (2000) 241–248.
[4] J. Halász, M. Hodos, I. Hannus, G. Tasi, I. Kiricsi, Colloids Surf. A 265 (2005) 171–177.
[5] R. López-Fonseca, P. Steltenpohl, J.R. González-Velasco, A. Aranzabal, J.I. Gutiérrez-Ortiz, Stud. Surf. Sci. Catal. 130 (2000) 893–898.
[6] L. Intriago, E. Díaz, S. Ordóñez, A. Vega, Micropor. Mesopor. Mater. 91 (2006) 161–169.
[7] S. Chatterjee, H.L. Greene, Y.J. Park, Catal. Today 11 (1992) 569–596.
[8] M. Guisnet, L. Costa, F.R. Ribeiro, J. Mol. Catal. A 305 (2009) 69–83.
[9] S. Chatterjee, H.L. Greene, J. Catal. 130 (1991) 76–85.
[10] R. López-Fonseca, J.I. Gutiérrez-Oritz, M.A. Gutiérrez-Ortiz, J.R. González-Velasco, J. Catal. 209 (2002) 145–150.
[11] R. López-Fonseca, S. Cibrián, J.I. Gutiérrez-Oritz, J.R. González-Velasco, Stud. Surf. Sci. Catal. 142 (2002) 847–854.
[12] M. Kraum, M. Baerns, Appl. Catal. A 186 (1999) 189–200.
[13] H. Kannisto, H.H. Ingelsten, M. Skoglundh, J. Mol. Catal. A 302 (2009) 86–96.
[14] S. Bhatia, A.Z. Abdulah, C.T. Wong, J. Hazard. Mater. 163 (2009) 73–81.
[15] Z. Mu, J.J. Li, H. Tian, Z.P. Hao, S.Z. Qiao, Mater. Res. Bull. 43 (2008) 2599–2606.
[16] H.L. Tidahy, S. Siffert, J.-F. Lamonier, R. Cousin, E.A. Zhilinskaya, A. Aboukaïs, B.-L. Su, X. Canet, G.D. Weireld, M. Frère, J.-M. Giraudon, G. Leclercq, Appl. Catal. B 70 (2007) 377–383.
[17] J.Z. Shyu, W.H. Weber, H.S. Gandhi, J. Phys. Chem. 92 (1988) 4964–4970.
[18] M.A. Kuehne, H.H. Kung, J.T. Miller, J. Catal. 171 (1997) 293–304.
[19] A. Hassan, S. Ahmed, M.A. Ali, H. Hamid, T. Inui, Appl. Catal. A 220 (2001) 59–68.
[20] M.M.R. Feijenn-Jeurissen, J.J. Jorna, B.E. Nieuwenhuys, G. Sinquin, C. Petit, J.-P. Hindermann, Catal. Today 54 (1999) 65–79.
[21] B. de Rivas, R. López-Fonseca, J.R. González-Velasco, J.I. Gutíerrez-Ortiz, J. Mol. Catal. A 278 (2007) 181–188.
[22] H.L. Greene, D.S. Prakash, K.V. Athota, Appl. Catal. B 7 (1996) 213–224.
[23] R. López-Fonseca, J.I. Gutiérrez-Ortiz, M.A. Gutiérrez-Ortiz, J.R. González-Velasco, J. Catal. 209 (2002) 145–150.
[24] J.M. Zhou, L. Zhao, Q.Q. Huang, R.X. Zhou, X.K. Li, Catal. Lett. 127 (2009) 277–284.
[25] J.I. Gutiérrez-Oritz, R. López-Fonseca, U. Aurrekoetxea, J.R. González-Velasco, J. Catal. 218 (2003) 148–154.
[26] T. Barzetti, E. Salli, D. Moscotti, L. Forni, J. Chem. Soc., Faraday Trans. 92 (1996) 1401–1407.
[27] B. Chakraborty, B. Viswanathan, Catal. Today 49 (1999) 253–260.
[28] J.A. Lercher, C. Gründling, G. Eder-Mirth, Catal. Today 27 (1996) 353–376.
[29] G. Busca, Catal. Today 41 (1998) 191–206.
[30] J.I. Gutiérrez-Ortiz, B. de Rivas, R. López-Fonseca, J.R. González-Velasco, Appl. Catal. A 269 (2004) 147–155.
[31] I. Atribak, A. Bueno-López, A. García-García, J. Catal. 259 (2008) 123–132.
[32] Y. Guo, G. Lu, Z. Zhang, S. Zhang, Y. Qi, Y. Liu, Catal. Today 126 (2007) 296–302.
[33] A. Aranzabal, J.A. González-Marcos, M. Romero-Sáez, J.R. González-Velasco, M. Guillemot, P. Magnoux, Appl. Catal. B 88 (2009) 533–541.
[34] E.G. Derouane, F. Lemos, C. Naccaciie, F. Ramoa-Riberio (Eds.), Zeolite Microporous Solids: Synthesis, Structure and Reactivity, Kulwer Academic Publishers, Dordrecht, The Netherlands, 1991, p. 457.
[35] M. Guisnet, P. Magnoux, Stud. Surf. Sci. Catal. 88 (1994) 53–68.
[36] A. Zuhairi, M. Zailani, S. Bhatia, React. Kinet. Catal. Lett. 79 (2003) 143–148.
[37] D.R. Mullins, S.H. Overbury, D.R. Huntley, Surf. Sci. 409 (1998) 307–319.
[38] P. Burroughs, A. Hamnett, A.F. Orchard, G. Thornton, J. Chem. Soc., Dalton Trans. 17 (1976) 1686–1698.
[39] D.A. Creaser, B.A. Wolfindale, Catal. Lett. 23 (1994) 13–24.
[40] Q.G. Dai, X.Y. Wang, G.Z. Lu, Appl. Catal. B 81 (2008) 192–202.
[41] M. Guillemot, J. Mijoin, S. Mignard, P. Magnoux, Appl. Catal. A 327 (2007) 211–217.
[42] S. Karmakar, H.L. Greene, J. Catal. 138 (1992) 364–376.
[43] G.M. Bickle, T. Suzuki, Y. Mitarai, Appl. Catal. B 4 (1994) 141–153.
[44] D.-P. Kim, J.-W. Yeo, C.-I. Kim, Thin Solid Films 459 (2004) 122–126.
[45] G. Praline, B.E. Koel, R.L. Hance, H.-I. Lee, J.M. White, J. Electron Spectrosc. Relat. Phenom. 21 (1980) 17–30.
[46] H.Y. Chen, A. Sayari, A. Adnot, F. Larachi, Appl. Catal. B 32 (2001) 195–204.